remote sensing

MDPI

Article

Evaluation of Hybrid Wavelet Models for Regional Drought Forecasting

Gilbert Hinge [1], Jay Piplodiya [2], Ashutosh Sharma [3], Mohamed A. Hamouda [4,5,*] and Mohamed M. Mohamed [4,5]

[1] Department of Civil Engineering, National Institute of Technology Durgapur, Durgapur 713209, West Bengal, India
[2] Department of Earth Sciences, Indian Institute of Technology Roorkee, Roorkee 247667, Uttarakhand, India
[3] Department of Hydrology, Indian Institute of Technology Roorkee, Roorkee 247667, Uttarakhand, India
[4] Department of Civil and Environmental Engineering, United Arab Emirates University, Al Ain P.O. Box 15551, United Arab Emirates
[5] National Water and Energy Center, United Arab Emirates University, Al Ain P.O. Box 15551, United Arab Emirates
* Correspondence: m.hamouda@uaeu.ac.ae

Abstract: Drought forecasting is essential for risk management and preparedness of drought mitigation measures. The present study aims to evaluate the effectiveness of the proposed hybrid technique for regional drought forecasting. Multiple Linear Regression (MLR), Artificial Neural Network (ANN), and two wavelet techniques, namely, Discrete Wavelet Transform (DWT) and Wavelet Packet Transform (WPT), were evaluated in drought forecasting up to a lead time of six months. Standard error metrics were used to select optimal model parameters, such as number of inputs, number of hidden neurons, level of decomposition, and number of mother wavelets. Additionally, the performance of various mother wavelets, including the Haar wavelet (db1) and 19 Daubechies wavelets (db1 to db20), were evaluated. The results indicated that the ANN model produced better forecasts than the MLR model, whereas the hybrid models outperformed both ANN and MLR models, which failed to predict the SPI values for a lead time greater than two months. The performance of all the models was found to improve as the timescale increased from 3 to 12 months. However, all the models' performances deteriorated as the lead time increased. The hybrid WPT-MLR was the best model for the study area. The findings indicated that a hybrid WPT-MLR model could be used for drought early warning systems in the study area.

Keywords: artificial neural network; drought; forecasting; India; multiple linear regression; wavelet

check for updates

Citation: Hinge, G.; Piplodiya, J.; Sharma, A.; Hamouda, M.A.; Mohamed, M.M. Evaluation of Hybrid Wavelet Models for Regional Drought Forecasting. *Remote Sens.* **2022**, *14*, 6381. https://doi.org/10.3390/rs14246381

Academic Editor: Yuei-An Liou

Received: 30 November 2022
Accepted: 13 December 2022
Published: 16 December 2022

Publisher's Note: MDPI stays neutral with regard to jurisdictional claims in published maps and institutional affiliations.

Copyright: © 2022 by the authors. Licensee MDPI, Basel, Switzerland. This article is an open access article distributed under the terms and conditions of the Creative Commons Attribution (CC BY) license (https://creativecommons.org/licenses/by/4.0/).

1. Introduction

Drought is one of the most catastrophic natural phenomena [1,2]. Drought is characterized by its duration, severity, and intensity [3]. Duration refers to how long the region is suffering from water deficit, while severity refers to the degree of water deficit. The ratio of severity to duration is known as the drought's intensity [4]. During the drought period, water supply is disrupted, agricultural yields are affected, environmental flows are reduced, and the socio-economic aspects of the people are being affected [5]. Drought prompts people to relocate, induces stress on human life, leading to starvation, and even triggers suicides [6,7]. Every year, millions of people are affected by drought in different parts of the world [8]. Over the last 150 years, India has suffered from 22 major drought events [9]. Many parts of India, particularly the arid and semi-arid regions, have suffered from recurrent drought in the past [1]. In recent years, the problem of drought has been further amplified due to increasing water demands and climate change [10,11]. Over the past few years, intensive research on drought has been carried out [6,12,13]. However, among all the different drought studies, drought forecasting is the most critical aspect of effective drought management.

Forecasting drought characteristics is essential for risk management and the preparedness of drought mitigation measures [14,15]. Several indices have been developed to quantify drought intensity. Some of the popular indices include Standardized Precipitation Index (SPI) [16], Standardized Precipitation Evapotranspiration Index (SPEI) [17], Palmer Drought Severity Index (PDSI) [18], Self-Calibrating Palmer Drought Severity Index (SC-PDCI) [19–21], and crop moisture index [22]. SPI is the most commonly used index among all these indices because of its easy computation and flexibility to compute for different time scales, making it possible to study any kind of drought [23]. Various researchers have used several time series and probabilistic models for drought forecasting using SPI and other drought indices [24]. For instance, Mishra and Desai [25] used two stochastic models, AutoRegressive Integrated Moving Average (ARIMA) and Seasonal ARIMA (SARIMA) for drought forecasting in the Kansabati river basin, India. Their models proved to be efficient in predicting drought up to two months ahead. Karavitis et al. [26] demonstrated the effectiveness of combining a stochastic model and a geospatial method for short-term drought prediction. Bazrafshan et al. [27] applied ARIMA for seasonal drought forecasting of the river basin in Iran. Han et al. [28] applied a remote sensing-based Vegetation Temperature Condition Index (VTCI) in northwest China for drought forecasting using the ARIMA model. Although these stochastic models are widely used for drought forecasting, they work on the assumption that the data is stationary, and therefore often fail to provide accurate forecasting for non-stationary and non-linear datasets.

Non-linear machine learning approaches such as Artificial Neural Networks (ANN), decision trees, and many others have been proposed to overcome stochastic models' limitations [29]. Since then, these techniques have been widely used for flood and drought forecasting. Mishra and Desai [30] used the Recursive Multi-Step Neural Network (RMSNN) for flood forecasting and compared their result with the same river basin as Mishra and Desai [25], which uses the linear stochastic model. Their results indicated that the RMSNN outperformed the stochastic model. Nguyen et al. [31] applied the Adaptive Neuro-Fuzzy Inference System (ANFIS) to predict drought using SPI and SPEI indices. They reported that their model provides accurate and reliable drought forecasting results. Further, the author concluded that SPI outperformed SPEI in predicting short-term droughts. Another application of ANN that was carried out in Iran by Morid et al. [32] predicted drought using SPI and Effective Drought Index (EDI). The best ANN models were reported with coefficient of determination values between 0.66 and 0.79 for a lead time of six months. Numerous machine learning algorithms for drought forecasting are available in the literature [6,33].

Despite the exciting advances of machine learning, recent studies have highlighted the inefficiency of most machine learning techniques to provide accurate prediction unless the data are preprocessed [34,35]. Therefore, it is crucial to perform data preprocessing before using machine learning models. Among the many available preprocessing techniques, Discrete Wavelet Transform (DWT) and Continuous Wavelet Transform (CWT) have been the most popular and widely used tool for preprocessing the hydrological and climatological data [36]. Wavelets are mathematical tools used to identify and separate the rapidly and slowly varying components of any time series [37]. In recent years, wavelet analysis has been tested for drought forecasting studies, where hydrological and meteorological long-term data are decomposed into rapidly and slowly detailed components and used as inputs for forecasting models [34,38]. Particularly the DWT and CWT were combined with various machine learning models to develop hybrid models to forecast droughts. Studies applying CWT-Linear Genetic Programming [39], DWT-ANN [34,38,40], and DWT-Support Vector Regression [41,42] are available in the literature. Recently, an emerging approach that considers the application of Wavelet Packet Transformation (WPT) as a more effective data preprocessing technique for drought modeling was tested. Das et al. [1] applied the WPT of SPI data and found that this processing helps in improving the model's performance in drought forecasting. On the contrary, the competence of WPT in preprocessing SPI data for drought forecasting has not been compared with DWT and CWT. In addition, while using wavelet, the selection of the mother wavelet and level of decomposition is very important [38]. However, most of the wavelet studies in drought analysis considered only the Haar (db1) mother wavelet. Very few studies have explored the response of various vanishing moments of Daubechies wavelets in drought prediction [38]. Hence, the present study, for the first time, aims to compare the benefits of DWT against WPT to enhance the drought forecasting performance of machine learning and linear models. Six different models, namely, a multiple regression model, a machine learning model (ANN), and four hybrid models were established for each station to forecast drought with a lead time of up to six months and for three different time scales (−3, −6, −12).

2. Study Area and Data Collection

2.1. Study Area

India has encountered many droughts in the past, particularly in the western part of the country. The study was conducted in the state of Rajasthan, which lies in the western part of India with a geographical extent between latitude of 21°–30°N and longitude of 72–78°E (Figure 1). The climate of the study area ranges from arid to semi-arid. As per the Koppen climate classification [43], most of the study area falls under Hot Desert (BWh) and a small portion under Hot Semi-Arid (BSh). This makes the study area highly prone to drought. The study area is characterized by low and erratic rainfall. The mean annual rainfall in the east and west part of the study area is approximately 64.9 and 32.7 cm, respectively [44]. Per the 2011 census, Rajasthan has a population of approximately 68 million, of which 75 percent live in rural areas and depend on rain for farming activities [45]. The northern part of the study area is covered by a desert ecosystem known as Thar desert. Aravalli is the oldest mountain range in the study area, and it affect the climatic and physiographic conditions [45]. One hundred and twenty-three India Meteorological Department (IMD) rainfall grid points spread over the study area are shown in Figure 1. This dataset is of 0.5° × 0.5° resolution and was developed for meteorological studies over the Indian region [46]. It was developed using controlled rainfall data from more than 6000 rain gauge stations [46].

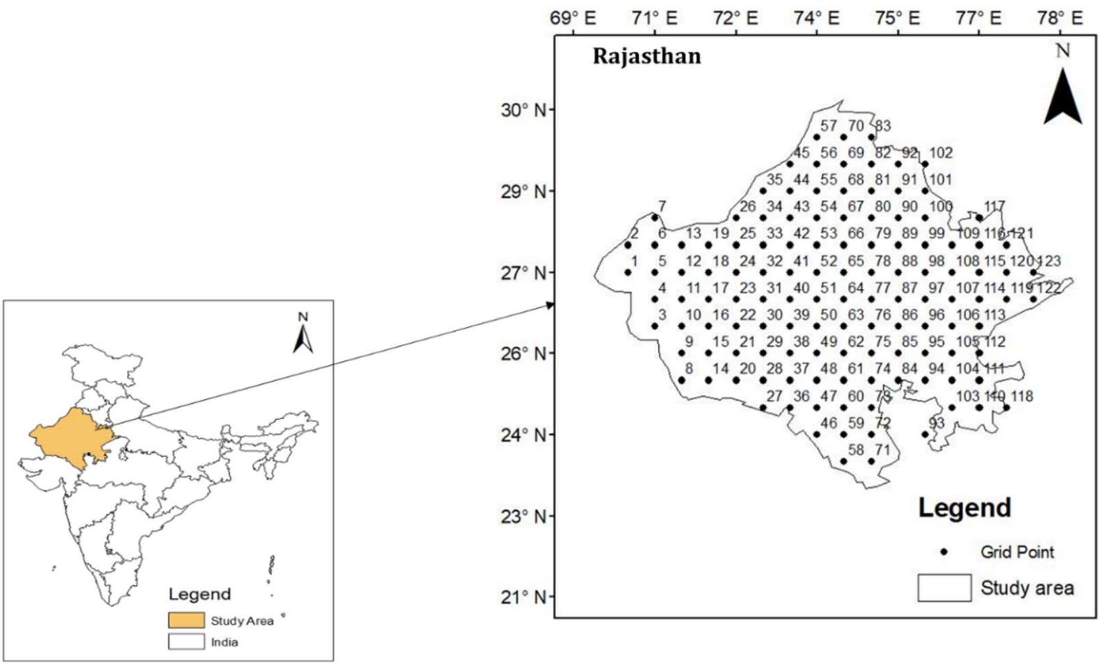

Figure 1. Location of study area (Rajasthan) and 123 Indian Meteorological Department grid points.

2.2. Data Collection

The present study used monthly rainfall data over 115 years, which were acquired from the India Meteorological Department (IMD) (http://www.imd.gov.in, accessed on 17 February 2022). The time series of the data was from January 1901 to December 2015. Details of the grid points can be found in the Supplementary Materials, Table S1. Before analysis, the homogeneity of rainfall data for each grid point was checked using the double mass technique. The accumulation of annual rainfall of each grid point was plotted against the accumulation of average annual rainfall of all the remaining grid points during the same period. Inconsistencies in rainfall data were corrected as per the method suggested by Adane et al. [47] Out of the 115 years of available data, the first 70 years were used to train the models, and the remaining years were used to test the models.

3. Methods

The overall methodology is divided into five steps—(1) Generation of SPI time series for three different time scale, (2) Study of lagged correlation of SPI index, (3) Formulation of standard models considering the lagged information of SPI to predict drought forecast up to six months lead time, (4) Decomposition of original SPI series into detailed and approximate components using WPT and DWT and formulation of hybrid model, (5) Evaluation and comparison of the model. The overview of the methodology is shown in Figure 2. Details of each of these modules are elaborated in the subsections below.

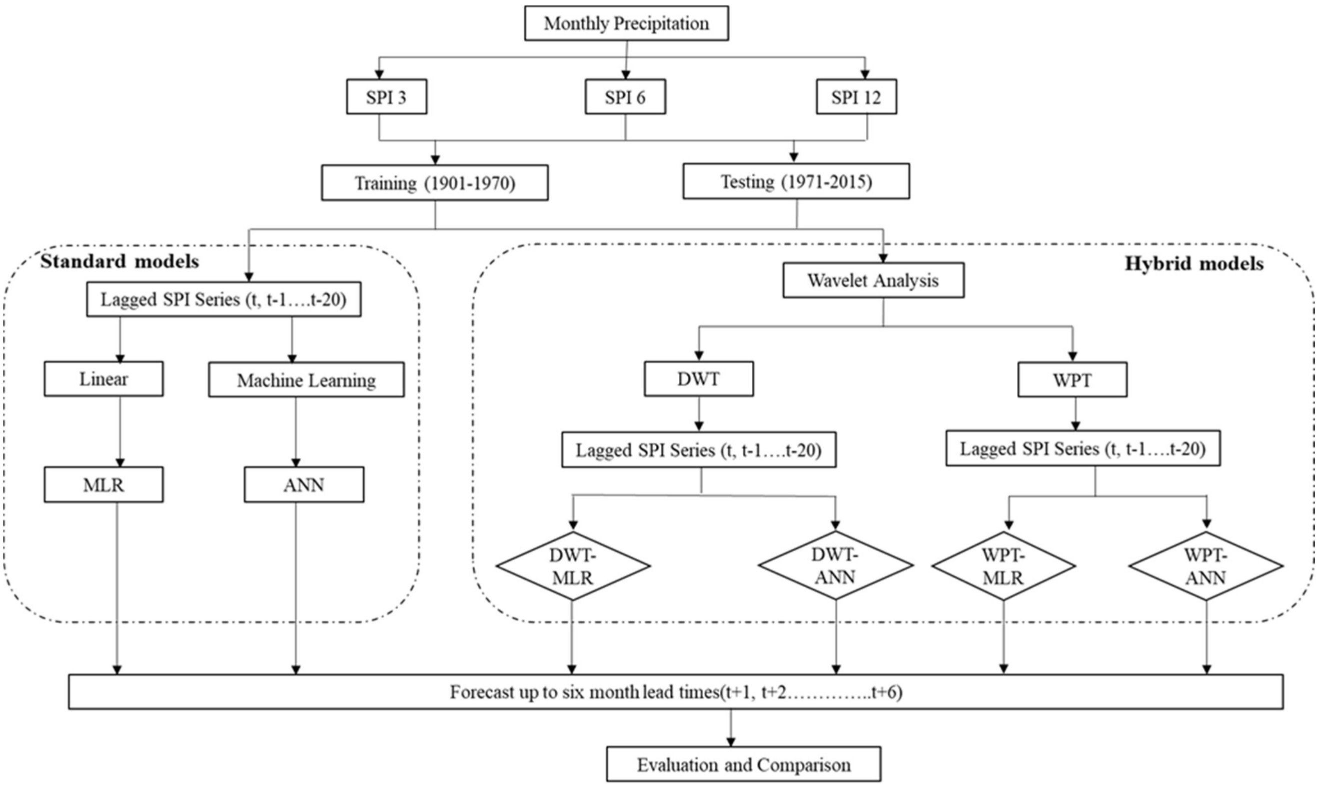

Figure 2. Overview of the methodology adopted in the present study. (SPI: Standard Precipitation Index, DWT: Discrete Wavelet Transform, MLR: Multiple Linear Regression, ANN: Artificial Neural Network, WPT: Wavelet Packet Transform).

3.1. Standard Precipitation Index (SPI)

The Standard Precipitation Index (SPI) was developed by Mckee et al. [16]. It has been endorsed by the World Meteorological Organization (WMO) as the main drought index for monitoring and quantification of drought intensity [48]. Through SPI, drought conditions of any area for different time scales such as 1, 3, 6, 12, 24, or 48 months can be calculated. Henceforth, it is possible to quantify meteorological and agricultural droughts that respond to rainfall anomalies of a relatively short scale (1–5 months) and hydrological droughts that respond to a longer scale (6–24 months) using this single index [16]. However, it has shortcomings as it is based only on precipitation data, while drought is not related to precipitation only [10], but this makes it appropriate for regions with a shortcoming of hydro-meteorological datasets [12]. This index was calculated by fitting the long-term precipitation data into a mathematical distribution function. In the present study, the gamma distribution was the best fit mathematical distribution function based on Chi-square tests and the Kolmogorov–Smirnov (K–S) test. The fitted data are transformed into a standard normal distribution function to ensure that the mean SPI of the desired location of any time scale is zero. SPI is expressed as:

$$SPI_{ijk} = \frac{P_{ijk} - \overline{P}_{ijk}}{\sigma_{ijk}} \tag{1}$$

where P_{ijk} = rainfall value for pixel i during timeframe j for year k (in mm), $\overline{P}_{ijk}$ = mean value for pixel i during timeframe j over n years (in mm), σ_{ijk} = standard deviation of pixel i during month j over n years (in mm).

Table 1 shows the drought classification using SPI values. A drought event is defined by values of SPI < −1 [16].

Table 1. Drought Classification as per SPI values (modified from [16]).

SPI Value	Classification
>2	Extremely wet
1.50 to1.99	Very Wet
1.00 to1.49	Moderately wet
−0.99 to 0.99	Near Normal
−1.0 to −1.49	Moderately dry
−1.5 to −1.99	Severely dry
<−2.0	Extremely dry

3.2. Artificial Neural Network

The Artificial Neural Network (ANN) is an advanced mathematical tool based on the concept of a biological neural system [49]. The function of ANN can be compared to the human brain, having nodes connecting to one another [50]. Thus, ANN consists of several interlinked nodes called neurons, which are arranged into different layers, namely input layer, hidden layer, and output layer [49]. The nodes in one layer are linked to the nodes in the subsequent layers. Each node is assigned a "weight" that measures the nodes' strength. During model training, these weights are updated such that the inputs produce output as close as possible to the desired values. ANN is a widely used application; hence, it is not discussed in detail. For detail, the reader may refer to Brace et al. [51] and Chandwani et al. [52].

Many neural network algorithms are available for carrying out complex computational works. The present study used a three-layered feedforward ANN model, which is the most widely used in the field of hydrology [25]. The input nodes for the model were the lagged observations (i.e., the SPI values). The output nodes of the model were the predicted SPI values. One hidden layer was considered, with the number of neurons varying between 1 and 15. The number of inputs was varied from 1 to 20. The number of inputs and number of hidden neurons were optimized based on a trial-and-error approach. The tangent sigmoid was used as an activation function between the input and hidden layers, and linear activation was used as an activation function between the hidden and output layers.

3.3. Multiple Linear Regression Model

The Multiple Linear Regression (MLR) model is a statistical method that help develop a correlation between dependent and independent variables. MLR is a simple addition to basic Linear Regression. MLR assumed that the relationship between the dependent and independent variables is linear. The equation for MLR is as follows:

$$\overline{Y} = C_0 + C_1M_1 + C_2M_2 + C_3M_3 + \ldots + C_nM_n \quad (2)$$

where $\overline{Y}$ = predicted value of the dependent variable, $C_0 \ldots\ C_n$ = independent variables, $M_1 \ldots\ M_n$ = estimated regression coefficients.

This study's independent variables are the lagged SPI values, whereas the dependent variable is the predicted SPI values. More detail regarding MLR can be found in Tranmer and Elliot [53].

3.4. Wavelet

Similar to the conventional Fourier transforms, wavelets are a mathematical function widely used to analyze non-linear and non-stationary time series data [54]. However, unlike the Fourier transform, which gives only the frequency domain, wavelets are localized, both in time and frequency domain [55]. Thus, wavelets can capture abrupt changes, peak values, and change points and are therefore widely used in forecasting [40]. The idea of a wavelet is to segregate the time series data into little waves called "wavelets" of finite duration and zero mean [56] using a localized basic function called mother wavelet (ψ) and scaling function.

The general condition for (ψ) to be called a wavelet are:

$$\int_{-\infty}^{\infty} \mathrm{y}\ (\mathrm{x})dx = 0 \quad (3)$$

$$\int_{-\infty}^{\infty} |\mathrm{y}\ (\mathrm{x})dx|^2 = 1 \quad (4)$$

From the mother wavele, ψ, one can derive the smaller wavelet by varying the scaling and translation parameter using the equation as follow:

$$\psi_{\mathrm{a,b}}\ (\mathrm{t}) = \frac{1}{\sqrt{a}}\mathrm{y}\left(\frac{t-b}{a}\right),\ b \in R, a\ \in R,\ a \neq 0 \quad (5)$$

where ψ(t) = mother wavelet prototype, a, b = scaling and translation parameters, R = real number.

When the term $\psi_{\mathrm{a,b}}$ (t) satisfies Equation (5) for a finite energy signal, then the successive wavelet transform of f(t) is defined as:

$$\mathrm{W}_{\psi}\ \mathrm{f(a,b)} = \frac{1}{\sqrt{a}}\ \int_R^{\cdot} \mathrm{f(t)}\overline{\mathrm{y}}\left(\frac{t-b}{a}\right) \quad (6)$$

where $\overline{\mathrm{y(t)}}$ = complex conjugate function of y(t).

Wavelets can be broadly classified as Discrete Wavelet Transform (DWT) and Continuous Wavelet Transform (CWT). More detail regarding the types of wavelet can be found in Maheswaran and Khosa [57]. The present study used a DWT as it is recommended by various studies [58–60].

In the case of DWT, for a signal, x(t), the smoother version of the signal for different time scale is given by:

$$C_0(t) = x(t) \quad (7)$$

$$C_j(t) = \sum_{l=-\infty}^{\infty} h(l)c_j(t + 2^{j-1}\ l) \quad (8)$$

Here, j is the level of decomposition and h is the low pass filter. The detail component of the signal is obtained by subtracting the smoothed form of the signal from the coarser signal, as follows:

$$d_j(t) = c_{j-1}(t) - c_j(t) \tag{9}$$

Evolved from Discrete Wavelet Transform, Wavelet Packet Transform (WPT) has also been shown to effectively process the SPI data for drought modelling [1]. Discrete Wavelet Transforms and Wavelet Packet Transform are time-frequency tools that decompose the signal into coefficients of low-frequency components and high-frequency components at their first level of decomposition. The difference between these two methods is the way they further decompose the signals after the first level, as shown in Figure 3 [61]. In DWT, the data are fed into a pair of low pass and high pass filters and are then decomposed to give the approximation and detail component. The approximation components are again fed into the pair of low pass and high pass filters to generate another approximation and details component. This process continues until the desired decomposition level is reached. However, in the case of WPT, both the approximation and detail components are being fed at all levels, resulting in a richer analysis with greater computational load.

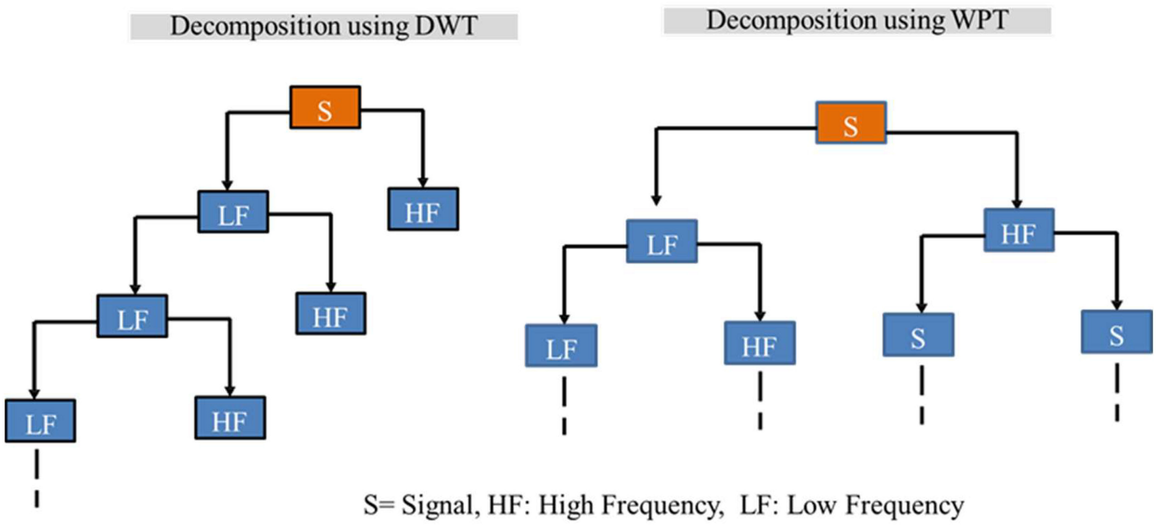

Figure 3. Difference between Discrete Wavelet Transform and Packet wavelet transform.

3.5. Model Development

The input signals (i.e., SPI series) were decomposed into detailed and smooth wavelet coefficients using DWT and WPT. These detailed coefficients served as an input for the MLR and ANN to develop hybrid DWT-MLR, DWT-ANN, WPT-MLR, and WPT-ANN models. Similar to the ANN and MLR models, the inputs for the hybrid models were the lagged coefficients, varying from one to six months based on minimum RMSE value. Codes were developed using MATLAB 2019a for implementing DWT and WPT. The choice of a suitable mother wavelet is an important step [37]. Hence, rather than using a particular mother wavelet, the present study evaluates all the Daubechies mother wavelets (from db1 to db20) and chooses the most appropriate wavelet for each station point based on the minimum RMSE value [37]. The optimum decomposition level for both DWT and WPT was selected based on the early stopping approach. Data from 1901 to 1970 were used for model training, and data from 1971 to 2015 were used for testing the models. The wavelet transform was performed separately for the training and testing datasets. Details of the different types of models for each station are shown in Table 2.

Table 2. Description of different types of models.

Model	Model Description
MLR	$SPI_i(t+T) = f_{MLR,i}(SPI_i(t-1), SPI_i(t-2), \ldots, SPI_i(t-L))$
ANN	$SPI_i(t+T) = f_{ANN,i}(SPI_i(t-1), SPI_i(t-2), \ldots, SPI_i(t-L))$
DWT-MLR	$SPI_i(t+T) = f_{DWT\_MLR,i}(DWT_{SPI,i}(t-1), DWT_{SPI,i}(t-2), \ldots, DWT_{SPI,i}(t-L))$ where $DWT_{SPI,i}(t-1) = [D_{SPI,i}, A_{SPI,i}]$
DWT-ANN	$SPI_i(t+T) = f_{DWT\_ANN,i}(DWT_{SPI,i}(t-1), DWT_{SPI,i}(t-2), \ldots, DWT_{SPI,i}(t-L))$ where $DWT_{SPI,i}(t-1) = [D_{SPI,i}, A_{SPI,i}]$
WPT-MLR	$SPI_i(t+T) = f_{WPT\_MLR,i}(WPT_{SPI,i}(t-1), WPT_{SPI,i}(t-2), \ldots, WPT_{SPI,i}(t-L))$ where $WPT_{SPI,i}(t-1) = [D_{SPI,i}, A_{SPI,i}]$
WPT-ANN	$SPI_i(t+T) = f_{WPT\_ANN,i}(WPT_{SPI,i}(t-1), WPT_{SPI,i}(t-2), \ldots, WPT_{SPI,i}(t-L))$ where $WPT_{SPI,i}(t-1) = [D_{SPI,i}, A_{SPI,i}]$

i: Stations, t: time period, T: lead time [1–6], L: optimum number of lags [1–20], SPI: Standardized Precipitation Index, D: Detail component, A: Approximation component, DWT: Discrete Wavelet Transform, MLR: Multiple Linear Regression, ANN: Artificial Neural Network, WPT: Wavelet Packet Transform.

3.6. Performance Measures

The forecasting performance of all the models for all 123 grid points was assessed with two statistical indices: Root Mean Square Error (RMSE) and Nash–Sutcliffe Efficiency (NSE). They are defined as follows:

Root Mean Square Error (RMSE):

$$\text{RMSE} = \sqrt{\frac{1}{n}\sum_{i=1}^{n}(f_i - y_i)^2} \tag{10}$$

Nash–Sutcliffe efficiency (NSE):

$$\text{NSE} = 1 - \frac{\frac{1}{n}\sum_{i=1}^{n}(f_i - y_i)^2}{\frac{1}{n}\sum_{i=1}^{n}(y_i - \overline{y})^2} \tag{11}$$

Mean Absolute Error

$$(\text{MAE}) = \frac{\sum_{i=1}^{n}|(f_i - y_i)|}{\text{n}} \tag{12}$$

where y_i = observed data series, f_i = estimated series, and $\overline{y}$ = average value of the data series.

4. Results and Discussion

4.1. Artificial Neural Network Model

4.1.1. Selection of Artificial Neural Network Parameters

The performance of the ANN model depends on the selection of hyperparameters, namely the number of hidden neurons and the number of inputs. The optimal hyperparameters were chosen for the present study based on the minimum RMSE value. The number of inputs (SPI lagged values) were varied from 1 to 20, and the number of hidden neurons was varied from 1 to 15. As the number of ANN parameters increases, the model complexity also increases, which results in over-fitting. Hence, to avoid over-fitting, the present study used an early stopping technique.

An example of ANN parameter selection for station 4 (Lat = 26.5, Long = 70.5) of a three-month times scale (SPI-3) is shown in Figure 4. Figure 4a shows the variation in RMSE with different numbers of inputs, whereas Figure 4b shows the variation in RMSE with the different number of neurons. From Figure 4a, the RMSE value starts decreasing when the number of inputs varies from 1 to 3, but after three inputs, the RMSE starts increasing again. Because RMSE increased after three inputs, the number of inputs were chosen as three for this station. Similarly, because RMSE increased after nine neurons, nine neurons were selected for this station (Figure 4b). It should be noted that this procedure was adopted to avoid overfitting the ANN model. A similar procedure was performed for all stations and for all time scales. Table S2 in the Supplementary Materials the optimum number of inputs and neurons for a different timescale for one month lead time. Similar results were obtained for all lead times.

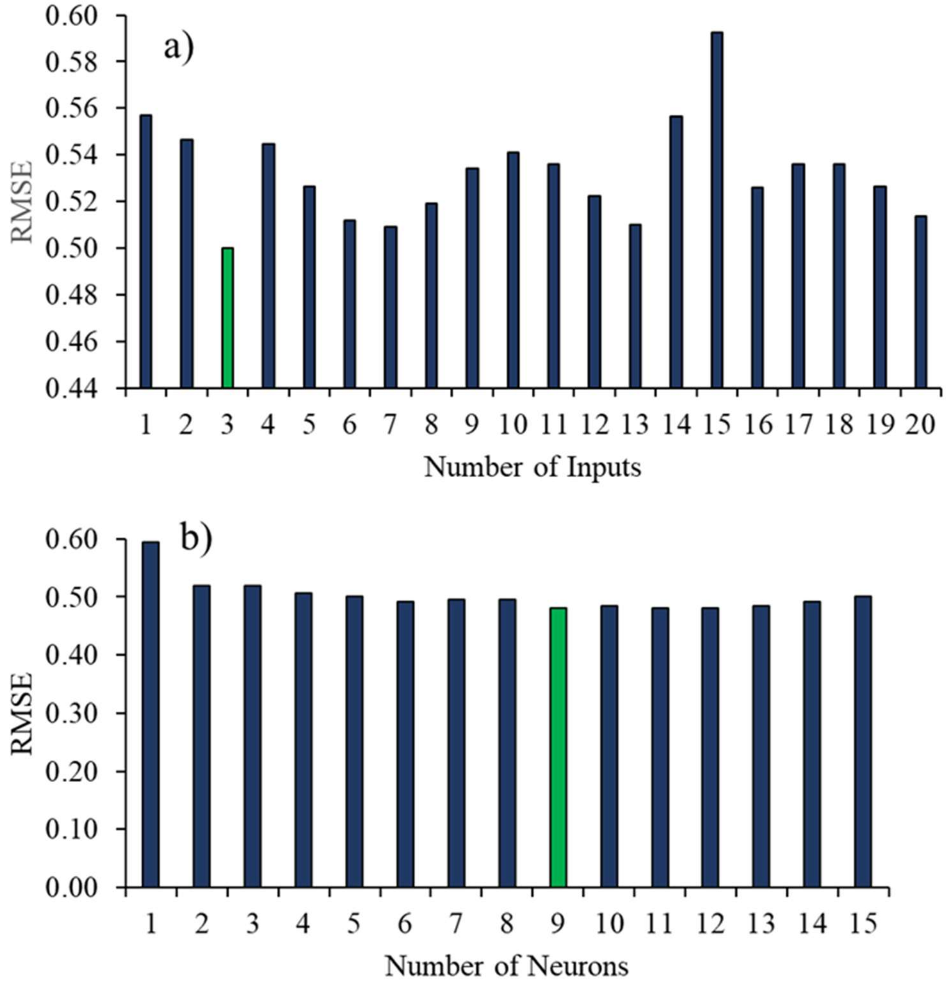

Figure 4. Sample selection of (**a**) input and (**b**) hidden neuron for grid point 4 (refer to Figure 1) SPI-3 ANN model.

4.1.2. Performance of Artificial Neural Network Model

The validation performance of the ANN model in forecasting different time scales over a 1–6 months lead time for all the grid stations is presented in Table 3. The values in Table 3 are the median RMSE, MAE, and NSE values of all 123 grid points in the study area. The RMSE, MAE, and NSE values were computed by comparing actual SPI versus forecasted SPI values. The forecast performance of the ANN model over different lead times was seen to improve as the time scales increased from 3 months to 6 months and from 6 months to 12 months, respectively. NSE was between −0.19 and 0.4 for SPI-3, between −0.16 and 0.55 for SPI-6, and between 0.3 and 0.9 for SPI-12. RMSE and MAE showed a similar observation to NSE. It is worth mentioning that even though the ANN parameters were optimized separately for different cases, the ANN models failed (i.e., NSE < 0) to predict SPI series for a lead time of greater than two months, particularly for SPI-3 and SPI-6. NSE < 0 indicates that the observed mean value is better than the prediction value by the model.

Table 3. Performance of standalone models.

Lead Time (Months)	Statistic	ANN Model			MLR Model		
		SPI-3	SPI-6	SPI-12	SPI-3	SPI-6	SPI-12
1	RMSE	0.7	0.66	0.3	0.93	0.86	0.76
	NSE	0.4	0.55	0.9	0.3	0.49	0.59
	MAE	0.6	0.48	0.2	0.69	0.54	0.30
2	RMSE	0.9	0.85	0.5	1.23	0.58	0.54
	NSE	0.1	0.25	0.7	−0.11	0.44	0.58
	MAE	0.7	0.65	0.3	0.75	0.59	0.39
3	RMSE	1.01	0.95	0.7	1.32	0.72	0.62
	NSE	−0.10	0.08	0.5	−0.52	−0.42	0.32
	MAE	0.80	0.74	0.4	0.79	0.60	0.48
4	RMSE	1.09	0.99	0.70	1.37	0.73	0.70
	NSE	−0.12	−0.02	0.5	−0.59	−0.47	−0.16
	MAE	0.81	0.79	0.5	0.85	0.65	0.52
5	RMSE	1.10	1.03	0.8	1.45	0.77	0.75
	NSE	−0.17	−0.10	0.4	−1.27	−1.10	−0.67
	MAE	0.82	0.80	0.60	0.87	0.72	0.69
6	RMSE	1.29	1.07	0.8	1.59	0.78	0.74
	NSE	−0.19	−0.16	0.3	−1.28	−1.21	−0.71
	MAE	0.83	0.81	0.63	0.88	0.73	0.68

4.2. Performance of Multiple Linear Regression Model

The validation performance of the MLR model in forecasting different time scales over a 1–6 month lead time for all the grid stations is presented in Table 3. As seen from Table 3, the MLR model performed poorly compared to the ANN model. Similar to the ANN model, the MLR models failed (i.e., NSE < 0) to predict the SPI series for a lead time of greater than two months, particularly for SPI-3 and SPI-6. This shows that both the standalone models (ANN and MLR) might not be able to predict extreme drought events for a greater lead time. The MLR model's performance was similar to the ANN model, which was also found to improve as the timescale increased from 3 to 12 months. RMSE was between 0.93 and 1.59 for SPI-3, between 0.87 and 1.43 for SPI-6, and between 0.72 and 1.30 for SPI-12. The values of NSE, MAE, and RMSE indicate that the performance of the MLR model consistently declined as the lead time increased.

4.3. Hybrid Models

4.3.1. Selection of Wavelet Parameters

The selection of wavelet parameters, namely the level of decomposition and mother wavelet, is a crucial step for the formation of hybrid models. For the present study, the level of decomposition varied from 1 to 6, and the mother wavelet from db1 to db20. The present study used the minimum RMSE value to select the best combination of mother wavelet and level of composition. An example of a method adopted for selecting wavelet parameters is shown in Table 4. The value in Table 4 represents the RMSE value for various combinations of mother wavelet and level of decomposition. The lowest RMSE value was found with a combination of dbn 12 and level of decomposition of 3. Hence, for this station, the value of dbn was chosen as 12 and the level of decomposition as 3. A similar procedure was performed for all stations, time scales, and lead times.

Table 4. Sample Selection of level of decomposition and mother wavelet based on minimum RMSE value. The chosen value is highlighted in bold.

		Mother Wavelet (dbn)																			
		1	2	3	4	5	6	7	8	9	10	11	12	13	14	15	16	17	18	19	20
Level of Decomposition	1	0.557	0.546	0.553	0.545	0.527	0.512	0.509	0.519	0.534	0.541	0.536	0.522	0.510	0.506	0.512	0.526	0.536	0.536	0.526	0.514
	2	0.540	0.517	0.521	0.520	0.491	0.480	0.491	0.496	0.495	0.512	0.504	0.481	0.482	0.487	0.482	0.494	0.508	0.496	0.489	0.488
	3	0.542	0.519	0.518	0.518	0.490	0.479	0.487	0.494	0.494	0.508	0.501	**0.478**	0.480	0.483	0.482	0.491	0.506	0.493	0.488	0.484
	4	0.542	0.519	0.518	0.518	0.492	0.479	0.487	0.495	0.494	0.509	0.501	0.479	0.480	0.484	0.482	0.491	0.506	0.494	0.488	0.484
	5	0.543	0.519	0.518	0.518	0.492	0.480	0.487	0.495	0.495	0.509	0.502	0.480	0.480	0.484	0.482	0.491	0.506	0.494	0.488	0.484
	6	0.544	0.519	0.518	0.519	0.492	0.480	0.487	0.496	0.495	0.509	0.502	0.480	0.480	0.484	0.482	0.491	0.506	0.494	0.488	0.484

Figure 5 shows the original SPI series for timescale 12 and its decomposed components for station 1. For illustration purposes, five levels of decomposition using mother wavelet dbn 7 is shown. It can be seen that the approximate component (*A*5) contains the low-frequency part, whereas the detail components (*D*1 to D5) contain the high-frequency components. A similar procedure was performed for all stations. These approximate and detailed components were used as an input into MLR and ANN models based on the optimum number of parameters for each station to form a hybrid model.

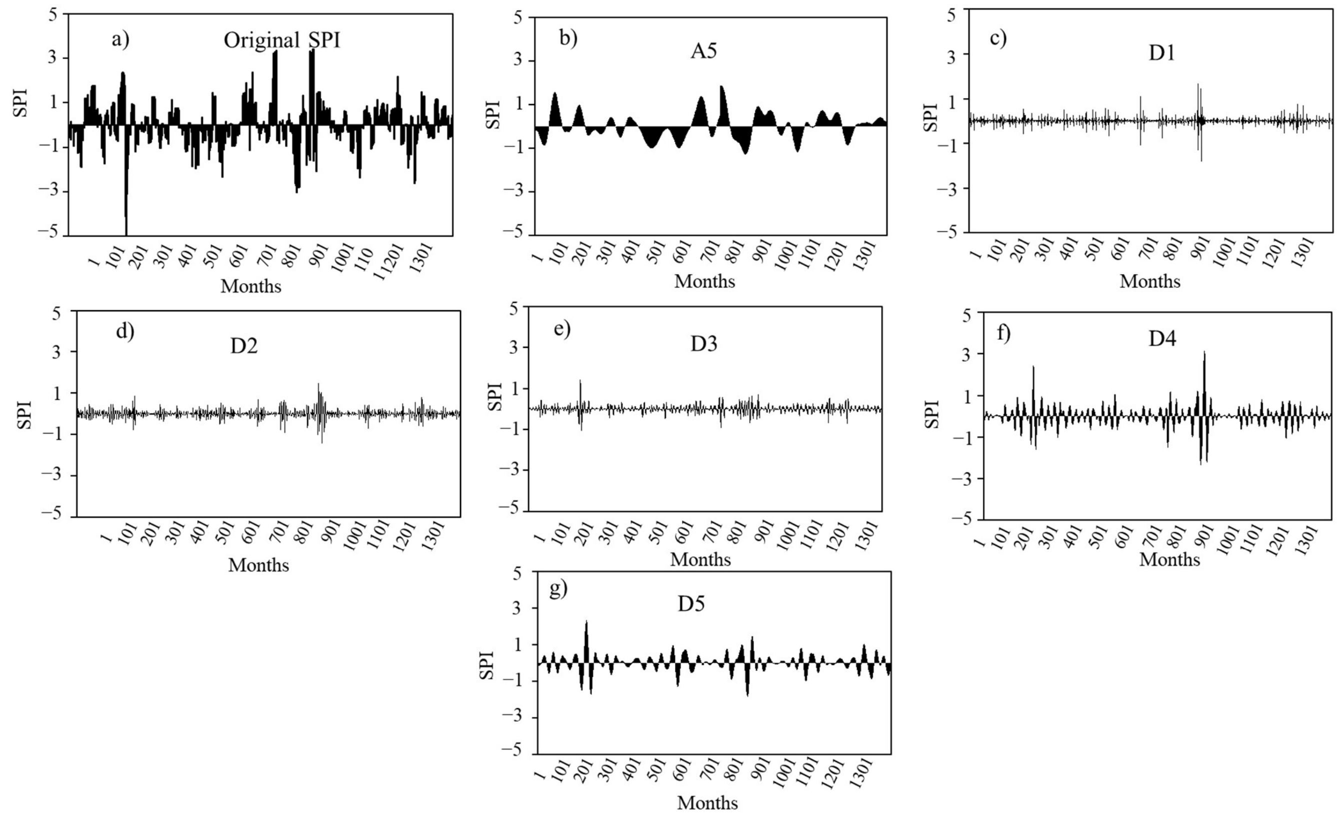

Figure 5. The change in SPI over the study period, where (**a**) represents the original SPI series for SPI-12 and (**b**–**g**) represent its respective decomposed approximate and detailed components for five levels of decomposition with mother wavelet dbn 7. The Y axis scale is kept the same to highlight the relative difference in the values of detailed and approximate components.

4.3.2. Performance of Hybrid Model

The validation performance of hybrid models, namely DWT-MLR, WPT-MLR, DWT-ANN, and WPT-ANN for SPI-3, SPI-6, and SPI-12 are shown in Table 5. It was observed that the hybrid models outperformed both the standalone models for all lead time periods (refer to Tables 3 and 5). For example, in the case of SPI-3, the RMSE of the ANN and MLR models for a lead time of 1 month were as high as 0.7 and 0.93 (Table 3), whereas the RMSE of DWT-ANN and WPT-ANN for SPI-3 with a 1 month lead time were 0.28 and 0.26, respectively (Table 5). Similarly, the NSE value of DWT-ANN and WPT-ANN for SPI-3 with a 6 month lead times were 0.30 and 0.82, respectively, compared to −0.19 and −1.28 in the standalone ANN and MLR models. The same trend was observed in the case of MAE value. This is likely because of the processing of the input with wavelet decomposition. The input pre-processing helps remove noise in the input data series, leading to better forecasting performance [62].

Table 5. Performance of hybrid models.

Lead Time (Months)	Statistic	SPI-3				SPI-6				SPI-12			
		DWT-MLR	WPT-MLR	DWT-ANN	WPT-ANN	DWT-MLR	WPT-MLR	DWT-ANN	WPT-ANN	DWT-MLR	WPT-MLR	DWT-ANN	WPT-ANN
1	RMSE	0.56	0.17	0.28	0.26	0.76	0.04	0.22	0.15	0.83	0.03	0.19	0.13
	NSE	0.49	0.97	0.91	0.93	0.59	1	0.95	0.95	0.84	1	0.96	0.98
	MAE	0.21	0.07	0.18	0.15	0.19	0.05	0.13	0.13	0.17	0.03	0.10	0.12
2	RMSE	0.58	0.09	0.49	0.25	0.54	0.03	0.46	0.23	0.77	0.03	0.3	0.17
	NSE	0.44	0.99	0.7	0.93	0.58	1	0.78	0.95	0.81	1	0.9	0.97
	MAE	0.22	0.08	0.19	0.17	0.25	0.06	0.19	0.15	0.21	0.04	0.13	0.13
3	RMSE	0.72	0.11	0.6	0.26	0.62	0.05	0.55	0.26	0.43	0.03	0.40	0.22
	NSE	−0.42	0.99	0.6	0.92	0.32	1	0.67	0.93	0.71	1	0.82	0.95
	MAE	0.25	0.08	0.23	0.18	0.27	0.07	0.23	0.16	0.23	0.05	0.18	0.14
4	RMSE	0.73	0.13	0.70	0.31	0.70	0.07	0.64	0.3	0.48	0.04	0.40	0.23
	NSE	−0.47	0.98	0.5	0.89	−0.16	0.99	0.57	0.91	0.67	1	0.8	0.94
	MAE	0.32	0.09	0.27	0.19	0.28	0.08	0.29	0.17	0.28	0.07	0.19	0.15
5	RMSE	0.77	0.2	0.70	0.38	0.75	0.11	0.70	0.35	0.57	0.07	0.40	0.28
	NSE	−1.10	0.95	0.4	0.84	−0.67	0.99	0.52	0.87	0.46	0.99	0.79	0.91
	MAE	0.36	0.10	0.28	0.19	0.29	0.09	0.30	0.18	0.28	0.08	0.20	0.17
6	RMSE	0.78	0.2	0.80	0.4	0.74	0.14	0.76	0.39	0.63	0.09	0.50	0.32
	NSE	−1.21	0.96	0.30	0.82	−0.71	0.98	0.41	0.84	0.25	0.99	0.70	0.89
	MAE	0.38	0.10	0.29	0.20	0.30	0.09	0.30	0.19	0.29	0.08	0.20	0.18

Another interesting observation is that the WPT hybrid models outperformed the DWT hybrid models for all lead times and time scales. Unlike DWT, in the case of WPT, both the detail and approximation components are further decomposed, resulting in richer analysis, with relatively low generalization error and better forecasting performance [1]. The present studies' findings are consistent with other studies that reported an improvement in the forecasting of the machine learning model when integrated with wavelets [1,38,62] These findings highlight the importance of pre-processing the SPI data before applying any machine learning for drought forecasting. The finding also indicated the superiority of WPT over DWT.

Similar to the forecasting performance of the standalone model, the performance of hybrid models decreased when the lead time was increased from 1 month to 6 months. Figure 6 shows the performance pertaining to the SPI-3 forecast under different lead times for both standalone and hybrid models. It is worth noting that the wavelet parameters were optimized separately for different cases; however, the DWT-MLR model still failed (i.e., NSE < 0) to predict SPI series for a lead time of greater than two months. However, in the case of DWT-ANN, the NSE value was above 0.5 up to a lead time of four months and went into negative values after a lead time of four. This indicates that the DWT processing technique works better with ANN than with the MLR model.

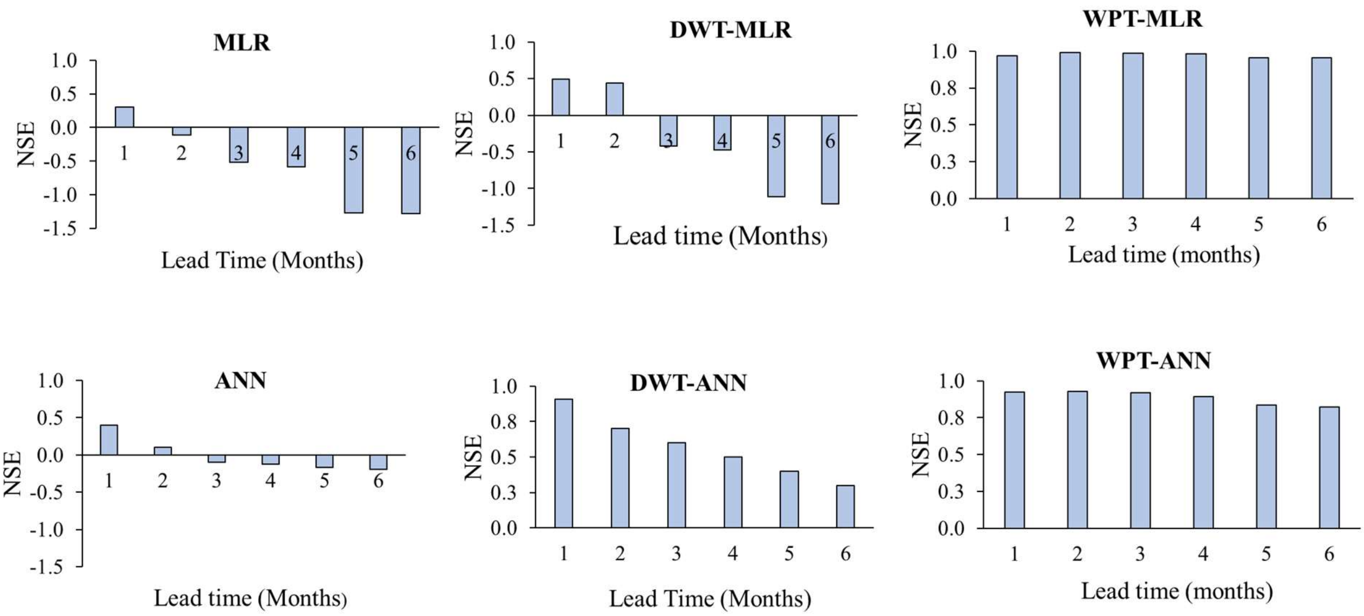

Figure 6. Different model's performance pertaining to SPI-3 forecast under different lead times.

Interestingly, the NSE of both WPT hybrid models (WPT-MLR and WPT-ANN) is above 0.5 for all lead time periods. RMSE exhibits the same behavior, with slightly less magnitude (Table 5). In the case of WPT-MLR, the NSE values of lead time two and lead times three were even better than the earlier lead times, indicating the promising potential of the WPT-MLR model to forecast drought for any lead time. Interestingly, in the case of the WPT model, WPT-MLR outperformed the WPT-ANN model. The reason for this may be due to the simplicity and reduced computation time of MLR compared to ANN, as the WPT results in a huge amount of data of decomposed components, which were used for training and testing the model. The WPT-MLR was the best model in forecasting SPI for all lead time periods and time scales.

Figure 7 shows the comparison of the performance of both standalone and hybrid models under different scales for different lead times. Similar to the standalone models, the performance of the hybrid models improved as the timescale increased from 3 to 6 months and, further, from 6 to 12 months. This is because the SPI-12 is not sensitive to changes in precipitation values from one month to the other months compared to SPI-3 and SPI-6 [1]. Thus, SPI of longer accumulation periods is easy to forecast compared to shorter accumulation periods. In general, the SPI-12 forecast provides a better forecast for all lead months.

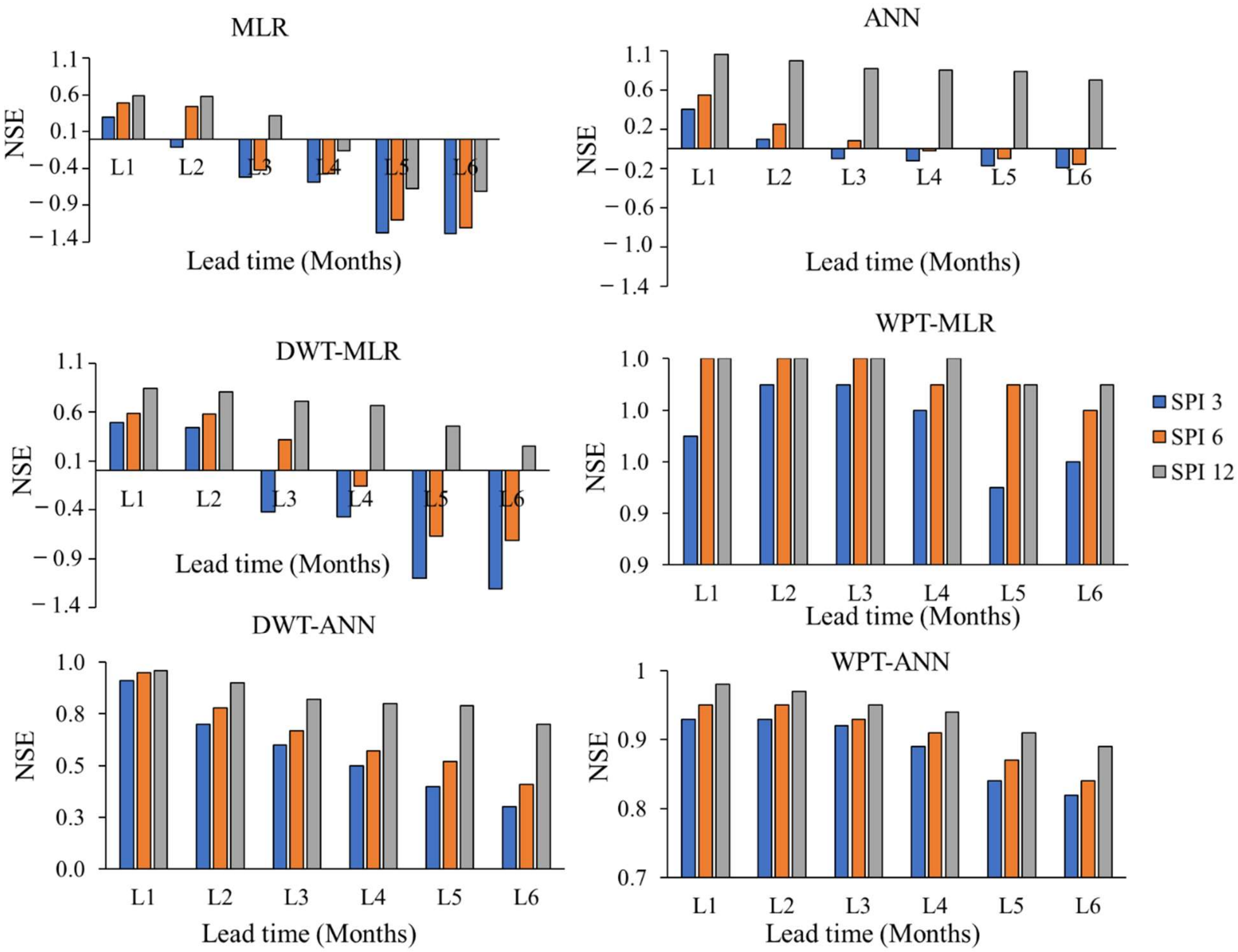

Figure 7. Performance of the models under different scales for different lead times.

5. Conclusions

An early indication of drought can assist in drought preparedness and mitigation. The present study evaluated two data pre-processing techniques, a linear model and a machine learning approach, to forecast drought in Rajasthan, India. The SPI index was used as a drought measure due to its advantages over other indices and ease of calculating different time scales. SPI-3, SPI-6, and SPI-12 were calculated and then forecast using MLR, ANN, hybrid MLR-DWT, MLR-WPT, ANN-DWT, and ANN-WPT for a lead time of up to 6 months. The MLR-WPT model was found to be the most effective model based on three performance statistics, namely MAE, NSE, and RMSE. MLR-WPT consistently showed lower RMSE, MAE, and NSE values, particularly for SPI-12 compared to all the other models used in this study. This indicates that the pre-processing of SPI time series resulted in the removal of noise, which improved the forecasting ability of the ANN and MLR models. The WPT, unlike other methods of data processing, helps to decompose the data into many folds, resulting in richer analysis and capturing helpful information. However, the WPT results in greater computation time, which may be the reason that MLR is a simpler model than ANN when combined with WPT. Thus, future studies should focus on testing the effectiveness of WPT for drought forecasting performance with different simpler and complex models.

Supplementary Materials: The following are available online at https://www.mdpi.com/article/10.3390/rs14246381/s1, Table S1: Geographical and rainfall statistics of IMD stations in the study area, Table S2: Optimal number of inputs and neurons chosen for the ANN model for 1 month lead time.

Author Contributions: Conceptualization, G.H., A.S., M.A.H. and M.M.M.; data curation, G.H. and A.S.; formal analysis, G.H., J.P. and A.S.; funding acquisition, M.M.M. and M.A.H.; investigation, G.H.; methodology, G.H. and A.S.; supervision, A.S., M.A.H. and M.M.M.; validation, A.S. and M.A.H.; visualization, G.H.; writing—original draft, G.H.; review and editing, A.S., M.A.H. and M.M.M. All authors have read and agreed to the published version of the manuscript.

Funding: This research was funded by the National Water and Energy Center, United Arab Emirates University through the Asian University Alliance (AUA) program, grant numbers 31R281-AUA-NWEC-4-2020, 12R023-AUA- NWEC -4- 2020, and 12R019-NWEC-6-2020.

Data Availability Statement: The data used in this study are freely available from the Indian Meteorological Department (IMD) website.

Conflicts of Interest: The authors declare no conflict of interest.

References

1. Das, P.; Naganna, S.R.; Deka, P.C.; Pushparaj, J. Hybrid wavelet packet machine learning approaches for drought modeling. *Environ. Earth Sci.* **2020**, *79*, 221. [CrossRef]
2. Chang, S.; Chen, H.; Wu, B.; Nasanbat, E.; Yan, N.; Davdai, B. A practical satellite-derived vegetation drought index for arid and semi-arid grassland drought monitoring. *Remote Sens.* **2021**, *13*, 414. [CrossRef]
3. Aksoy, H.; Cetin, M.; Eris, E.; Burgan, H.I.; Cavus, Y.; Yildirim, I.; Sivapalan, M. Critical drought intensity-duration-frequency curves based on total probability theorem-coupled frequency analysis. *Hydrol. Sci. J.* **2021**, *66*, 1337–1358. [CrossRef]
4. Sun, P.; Ma, Z.; Zhang, Q.; Singh, V.P.; Xu, C.-Y. Modified drought severity index: Model improvement and its application in drought monitoring in China. *J. Hydrol.* **2022**, *612*, 128097. [CrossRef]
5. Mishra, A.K.; Desai, V.R. Drought forecasting using feed-forward recursive neural network. *Ecol. Modell.* **2006**, *198*, 127–138. [CrossRef]
6. de Brito, C.S.; da Silva, R.M.; Santos, C.A.G.; Neto, R.M.B.; Coelho, V.H.R. Monitoring meteorological drought in a semiarid region using two long-term satellite-estimated rainfall datasets: A case study of the Piranhas River basin, northeastern Brazil. *Atmos. Res.* **2021**, *250*, 105380. [CrossRef]
7. Rousta, I.; Olafsson, H.; Moniruzzaman, M.; Zhang, H.; Liou, Y.-A.; Mushore, T.D.; Gupta, A. Impacts of drought on vegetation assessed by vegetation indices and meteorological factors in Afghanistan. *Remote Sens.* **2020**, *12*, 2433. [CrossRef]
8. Goyal, M.K.; Sharma, A. A fuzzy c-means approach regionalization for analysis of meteorological drought homogeneous regions in western India. *Nat. Hazards* **2016**, *84*, 1831–1847. [CrossRef]
9. Samra, J.S. *Review and Analysis of Drought Monitoring, Declaration and Management in India*; IWMI: Colombo, Sri Lanka, 2004; Volume 84, ISBN 929090576X.
10. Hinge, G.; Mohamed, M.M.; Long, D.; Hamouda, M.A. Meta-Analysis in Using Satellite Precipitation Products for Drought Monitoring: Lessons Learnt and Way Forward. *Remote Sens.* **2021**, *13*, 4353. [CrossRef]
11. Aghelpour, P.; Bahrami-Pichaghchi, H.; Varshavian, V. Hydrological drought forecasting using multi-scalar streamflow drought index, stochastic models and machine learning approaches, in northern Iran. *Stoch. Environ. Res. Risk Assess.* **2021**, *35*, 1615–1635. [CrossRef]
12. Pai, D.S.; Sridhar, L.; Guhathakurta, P.; Hatwar, H.R. District-wide drought climatology of the southwest monsoon season over India based on standardized precipitation index (SPI). *Nat. Hazards* **2011**, *59*, 1797–1813. [CrossRef]
13. Hinge, G.; Sharma, A. Comparison of wavelet and machine learning methods for regional drought prediction. In Proceedings of the EGU General Assembly Conference Abstracts, Vienna, Austria, 23–27 May 2022; p. EGU21-218.
14. Jain, S.K.; Keshri, R.; Goswami, A.; Sarkar, A. Application of meteorological and vegetation indices for evaluation of drought impact: A case study for Rajasthan, India. *Nat. Hazards* **2010**, *54*, 643–656. [CrossRef]
15. Stahl, K.; Kohn, I.; Blauhut, V.; Urquijo, J.; De Stefano, L.; Acácio, V.; Dias, S.; Stagge, J.H.; Tallaksen, L.M.; Kampragou, E. Impacts of European drought events: Insights from an international database of text-based reports. *Nat. Hazards Earth Syst. Sci.* **2016**, *16*, 801–819. [CrossRef]
16. McKee, T.B.; Doesken, N.J.; Kleist, J. The relationship of drought frequency and duration to time scales. In Proceedings of the 8th Conference on Applied Climatology, Boston, MA, USA, 17–22 January 1993; Volume 17, pp. 179–183.
17. Vicente-Serrano, S.M.; Beguería, S.; López-Moreno, J.I. A multiscalar drought index sensitive to global warming: The standardized precipitation evapotranspiration index. *J. Clim.* **2010**, *23*, 1696–1718. [CrossRef]
18. Palmer, W.C. *Meteorological Drought*; US Department of Commerce, Weather Bureau: Washington, DC, USA, 1965; p. 58.
19. Dai, A.; Trenberth, K.E.; Qian, T. A global dataset of Palmer Drought Severity Index for 1870–2002: Relationship with soil moisture and effects of surface warming. *J. Hydrometeorol.* **2004**, *5*, 1117–1130. [CrossRef]
20. Mavromatis, T. Use of drought indices in climate change impact assessment studies: An application to Greece. *Int. J. Climatol.* **2010**, *30*, 1336–1348. [CrossRef]
21. Wells, N.; Goddard, S.; Hayes, M.J. A self-calibrating Palmer drought severity index. *J. Clim.* **2004**, *17*, 2335–2351. [CrossRef]

22. Palmer, W.C. Keeping track of crop moisture conditions, nationwide: The new crop moisture index. *Weatherwise* **1968**, *21*, 156–161. [CrossRef]
23. Guttman, N.B. Comparing the palmer drought index and the standardized precipitation index 1. *JAWRA J. Am. Water Resour. Assoc.* **1998**, *34*, 113–121. [CrossRef]
24. Mishra, A.K.; Singh, V.P. Drought modeling–A review. *J. Hydrol.* **2011**, *403*, 157–175. [CrossRef]
25. Mishra, A.K.; Desai, V.R. Drought forecasting using stochastic models. *Stoch. Environ. Res. Risk Assess.* **2005**, *19*, 326–339. [CrossRef]
26. Karavitis, C.A.; Vasilakou, C.G.; Tsesmelis, D.E.; Oikonomou, P.D.; Skondras, N.A.; Stamatakos, D.; Fassouli, V.; Alexandris, S. Short-term drought forecasting combining stochastic and geo-statistical approaches. *Eur. Water* **2015**, *49*, 43–63.
27. Bazrafshan, O.; Salajegheh, A.; Bazrafshan, J.; Mahdavi, M.; Fatehi Maraj, A. Hydrological drought forecasting using ARIMA models (case study: Karkheh Basin). *Ecopersia* **2015**, *3*, 1099–1117.
28. Han, P.; Wang, P.X.; Zhang, S.Y. Drought forecasting based on the remote sensing data using ARIMA models. *Math. Comput. Model.* **2010**, *51*, 1398–1403. [CrossRef]
29. Kigumi, J.M. Use of Earth Observation Data and Artificial Neural Networks for Drought Forecasting: Case Study of Narumoro Sub-Catchment. Ph.D. Thesis, Pan African University, Addis Ababa, Ethiopia, 2018.
30. Shah, H.L.; Mishra, V. Uncertainty and bias in satellite-based precipitation estimates over Indian subcontinental basins: Implications for real-time streamflow simulation and flood prediction. *J. Hydrometeorol.* **2016**, *17*, 615–636. [CrossRef]
31. Nguyen, L.B.; Li, Q.F.; Ngoc, T.A.; Hiramatsu, K. Adaptive Neuro–Fuzzy Inference System for Drought Forecasting in the Cai River Basin in Vietnam. *J. Fac. Agric. Kyushu Univ.* **2015**, *60*, 405–415. [CrossRef]
32. Morid, S.; Smakhtin, V.; Bagherzadeh, K. Drought forecasting using artificial neural networks and time series of drought indices. *Int. J. Climatol. A J. R. Meteorol. Soc.* **2007**, *27*, 2103–2111. [CrossRef]
33. Dai, A. Drought under global warming: A review. *Wiley Interdiscip. Rev. Clim. Chang.* **2011**, *2*, 45–65. [CrossRef]
34. Belayneh, A.; Adamowski, J.; Khalil, B.; Ozga-Zielinski, B. Long-term SPI drought forecasting in the Awash River Basin in Ethiopia using wavelet neural network and wavelet support vector regression models. *J. Hydrol.* **2014**, *508*, 418–429. [CrossRef]
35. Belayneh, A.; Adamowski, J.; Khalil, B. Short-term SPI drought forecasting in the Awash River Basin in Ethiopia using wavelet transforms and machine learning methods. *Sustain. Water Resour. Manag.* **2016**, *2*, 87–101. [CrossRef]
36. Kim, T.-W.; Valdés, J.B. Nonlinear model for drought forecasting based on a conjunction of wavelet transforms and neural networks. *J. Hydrol. Eng.* **2003**, *8*, 319–328. [CrossRef]
37. Maity, R.; Suman, M.; Verma, N.K. Drought prediction using a wavelet based approach to model the temporal consequences of different types of droughts. *J. Hydrol.* **2016**, *539*, 417–428. [CrossRef]
38. Djerbouai, S.; Souag-Gamane, D. Drought forecasting using neural networks, wavelet neural networks, and stochastic models: Case of the Algerois Basin in North Algeria. *Water Resour. Manag.* **2016**, *30*, 2445–2464. [CrossRef]
39. Mehr, A.D.; Kahya, E.; Özger, M. A gene–wavelet model for long lead time drought forecasting. *J. Hydrol.* **2014**, *517*, 691–699. [CrossRef]
40. Deo, R.C.; Tiwari, M.K.; Adamowski, J.F.; Quilty, J.M. Forecasting effective drought index using a wavelet extreme learning machine (W-ELM) model. *Stoch. Environ. Res. Risk Assess.* **2017**, *31*, 1211–1240. [CrossRef]
41. Belayneh, A.; Adamowski, J. Standard precipitation index drought forecasting using neural networks, wavelet neural networks, and support vector regression. *Appl. Comput. Intell. Soft Comput.* **2012**, *2012*, 794061. [CrossRef]
42. Komasi, M.; Sharghi, S.; Safavi, H.R. Wavelet and cuckoo search-support vector machine conjugation for drought forecasting using Standardized Precipitation Index (case study: Urmia Lake, Iran). *J. Hydroinform.* **2018**, *20*, 975–988. [CrossRef]
43. Peel, M.C.; Finlayson, B.L.; McMahon, T.A. Updated world map of the Köppen-Geiger climate classification. *Hydrol. Earth Syst. Sci.* **2007**, *11*, 1633–1644. [CrossRef]
44. Mundetia, N.; Sharma, D. Analysis of rainfall and drought in Rajasthan State, India. *Glob. Nest J* **2015**, *17*, 12–21.
45. Mishra, D.; Goswami, S.; Matin, S.; Sarup, J. Analyzing the extent of drought in the Rajasthan state of India using vegetation condition index and standardized precipitation index. *Model. Earth Syst. Environ.* **2022**, *8*, 601–610. [CrossRef]
46. Rajeevan, M.; Bhate, J. A high resolution daily gridded rainfall dataset (1971–2005) for mesoscale meteorological studies. *Curr. Sci.* **2009**, *96*, 558–562.
47. Adane, G.B.; Hirpa, B.A.; Song, C.; Lee, W.-K. Rainfall characterization and trend analysis of wet spell length across varied landscapes of the Upper Awash River Basin, Ethiopia. *Sustainability* **2020**, *12*, 9221. [CrossRef]
48. GUIDE; WMO Standardized Precipitation Index User; Svoboda, M.; Hayes, M.; Wood, D. *World Meteorological Organization: Geneva*; WMO: Geneva, Switzerland, 2012.
49. Agatonovic-Kustrin, S.; Beresford, R. Basic concepts of artificial neural network (ANN) modeling and its application in pharmaceutical research. *J. Pharm. Biomed. Anal.* **2000**, *22*, 717–727. [CrossRef] [PubMed]
50. Kukreja, H.; Bharath, N.; Siddesh, C.S.; Kuldeep, S. An introduction to artificial neural network. *Int. J. Adv. Res. Innov. Ideas Educ.* **2016**, *1*, 27–30.
51. Brace, M.C.; Schmidt, J.; Hadlin, M. Comparison of the forecasting accuracy of neural networks with other established techniques. In Proceedings of the First International Forum on Applications of Neural Networks to Power Systems, Singapore, 18-21 November 1991; pp. 31–35.

52. Chandwani, V.; Agrawal, V.; Nagar, R. Applications of soft computing in civil engineering: A review. *Int. J. Comput. Appl.* **2013**, *81*, 13–20. [CrossRef]
53. Tranmer, M.; Elliot, M. Multiple linear regression. *Cathie Marsh Cent. Census Surv. Res.* **2008**, *5*, 1–5.
54. Grossmann, A.; Morlet, J. Decomposition of Hardy functions into square integrable wavelets of constant shape. *SIAM J. Math. Anal.* **1984**, *15*, 723–736. [CrossRef]
55. Özger, M.; Mishra, A.K.; Singh, V.P. Long lead time drought forecasting using a wavelet and fuzzy logic combination model: A case study in Texas. *J. Hydrometeorol.* **2012**, *13*, 284–297. [CrossRef]
56. Kişi, Ö. Wavelet regression model as an alternative to neural networks for monthly streamflow forecasting. *Hydrol. Process. Int. J.* **2009**, *23*, 3583–3597. [CrossRef]
57. Maheswaran, R.; Khosa, R. Comparative study of different wavelets for hydrologic forecasting. *Comput. Geosci.* **2012**, *46*, 284–295. [CrossRef]
58. Joshi, N.; Gupta, D.; Suryavanshi, S.; Adamowski, J.; Madramootoo, C.A. Analysis of trends and dominant periodicities in drought variables in India: A wavelet transform based approach. *Atmos. Res.* **2016**, *182*, 200–220. [CrossRef]
59. Khan, M.M.H.; Muhammad, N.S.; El-Shafie, A. Wavelet based hybrid ANN-ARIMA models for meteorological drought forecasting. *J. Hydrol.* **2020**, *590*, 125380. [CrossRef]
60. Sharma, A.; Goyal, M.K. Assessment of drought trend and variability in India using wavelet transform. *Hydrol. Sci. J.* **2020**, *65*, 1539–1554. [CrossRef]
61. Rizal, A.; Hidayat, R.; Nugroho, H.A. Comparison of discrete wavelet transform and wavelet packet decomposition for the lung sound classification. *Far East J. Electron. Commun.* **2017**, *17*, 1065–1078. [CrossRef]
62. Nourani, V.; Baghanam, A.H.; Adamowski, J.; Kisi, O. Applications of hybrid wavelet–artificial intelligence models in hydrology: A review. *J. Hydrol.* **2014**, *514*, 358–377. [CrossRef]